A sequential model-based approach for gas turbine performance diagnostics

Chen, Yu-Zhi ; Zhao, Xu-Dong ; Xiang, Heng-Chao ; Tsoutsanis, Elias

DOI:
10.1016/j.energy.2020.119657

A sequential model-based approach for gas turbine performance diagnostics

Yu-Zhi Chen[1], Xu-Dong Zhao[2,*], Heng-Chao Xiang[3], Elias Tsoutsanis[4]
[*] Corresponding author (xdzhaohit@gmail.com)

ABSTRACT

The gradual degradation of gas turbine components is an inevitable result of engine operation, impacting engine availability, reliability, and operating cost. Gas path analysis plays an essential role in engine fault diagnosis. Accurate and fast diagnosis of multiple simultaneously degraded components has always posed a challenge, especially when the number of available measurements is limited. This paper proposes a novel performance diagnostic method that partitions the engine diagnosis into a series of steps to remove the "smearing effect" and reduce the matrix dimensions in the iterative diagnostic algorithm. An engine performance model of a triple-shaft gas turbine has been developed and validated against commercial software, in order to assess the accuracy and computational performance of the proposed method. The advantage of the proposed method lies in its capability to detect the severity of engine component degradation, such as compressor fouling and turbine erosion, with greater accuracy and computational efficiency than other model-based methods that use the same number of measurements. The newly developed method provides an accurate diagnosis with a reduced set of measurements. The method can deal effectively with the presence of random noise in the measurements and carries a significantly lower computation burden in comparison to existing methods. The proposed method could be used as a tool for supporting condition monitoring systems for improved gas turbine reliability and energy efficiency.

[1] Key Laboratory of Intelligent Control and Optimization for Industrial Equipment (Dalian University of Technology), Ministry of Education, Dalian 116024, China
[2] Key Laboratory of Intelligent Control and Optimization for Industrial Equipment (Dalian University of Technology), Ministry of Education, Dalian 116024, China
[3] China Gas Turbine Establishment, Aero Engine Corporation of China, Chengdu, 610500, China.
[4] Department of Mechanical Engineering, University of Birmingham, Edgbaston, Birmingham, B15 2TT, UK

Key Words: Gas Turbine Diagnostics; Gas Path Analysis; Model-Based Diagnostics; Gas Turbine Performance.

Nomenclature

CP	=	Characteristic parameter of component
$f(\cdot)$	=	Nonlinear vector-value function
FAR	=	Fuel-air ratio
FPT	=	Free power turbine
H	=	Enthalpy [kJ/kg]
HPC	=	High-pressure compressor
HPT	=	High-pressure turbine
LPC	=	Low-pressure compressor
LPT	=	Low-pressure turbine
n	=	Number of operating points
P	=	Total pressure [atm]
RH	=	Relative humidity [%]
$RMSE$	=	Root mean square error
S	=	Entropy [kJ/(kg·K)]
T	=	Total temperature [K]
W	=	Mass flow rate [kg/s]
WAR	=	Water-air ratio
X	=	Iteration variables, covers degradation factor variables
Z	=	Measurement parameter

Greek Letters

λ	=	Relative error of degradation factor as a percentage

ρ = Density [kg/m^3]

Subscripts

ac = Actual

CW = Compressor work

E = Efficiency

F = Flow capacity

L = Number of degradation factors

M = Number of measurement parameters

Mea = Measurement

pd = Predicted

PR = Pressure ratio

TW = Turbine work

1. Introduction

The pursuit of high reliability, availability, and efficiency in gas turbines has governed the evolution of engine maintenance methods [1]. Currently, the maintenance cost of the gas turbine is an important aspect of engine lifecycle expenditure. For instance, the lifecycle expenditure of the Siemens V94.3A gas turbine is expected to be 51.34 million Euros, which is 17.9 times the initial purchase cost of 2.86 million Euros, according to its 40-year life maintenance plan [2]. It is suggested that a more cost-efficient way of operating gas turbines could be achieved by enhanced engine condition monitoring and appropriate repairs [3,4]. Talebi and Tousi (2017) [5] demonstrated that gas path analysis (GPA), introduced by Urban (1969) [6], remains one of the soundest technologies for engine health monitoring and is widely used for gas turbine condition monitoring to detect, identify, and assess component degradation. This, in turn, affects the maintenance of gas turbine assets [7].

The degradation of gas turbine components has a great impact on the engine's loss of performance from both a thermodynamic and an economic perspective [8]. Some of the most common types of gas turbine degradation are fouling, erosion, corrosion, rubbing wear, hot section damage, seal damage, and object damage [9]. The types of deterioration fall into two classes: recoverable and unrecoverable [10]. Diagnostic methods are also classified into three categories: model-based, data-driven, and hybrid methods [11,12].

The diagnostic accuracy of model-based methods relies heavily on the gas turbine model, which requires extensive expert knowledge related to the model's development and presents a great challenge. On the other hand, data-driven approaches such as artificial neural networks [13], and deep learning [14], have excellent accuracy, subject to an extensive training phase. The latter methods are limited by identifying new sets of data that are not used in their training phase. A family of object-oriented Artificial Intelligence methods is also gaining significant ground in the engine diagnostics arena [10,15]. The hybrid approaches can address some, but definitely not all, of the above limitations by combining two or more methods. Thus, there are trade-offs in accuracy, computational performance, and measurement noise, to name only a few considerations when selecting a diagnostic method. However, real-time diagnosis is crucial for decision-making to ensure optimum, safe, and reliable engine operation. This study will focus on model-based approaches, which present greater challenges in terms of accuracy and computational speed, especially when such solutions are to be deployed in a real-time condition monitoring system.

The number of simultaneous fault components can profoundly affect the performance of the diagnosis [16,17]. When there are more than two degraded components, the complexity of nonlinear diagnostic systems is significantly increased [17]. Traditionally, the number of engine measurements should be larger than the number of health parameters to produce a unique diagnostic solution [1]. Hence, an increase in the number of engine components that can degrade will not only increase the number of health parameters but also increase the number of measurement parameters. In such a condition, two issues are raised for engine diagnosis: limited availability of engine measurements for predicting every health parameter correctly and an increase of the matrix dimensions, which reduces computational efficiency.

Regarding diagnostic accuracy, it has been pointed out that monitoring more degraded components using a limited number of measurements could cause a severe "smearing effect" and lead to low precision [16]. The "smearing effect" is the result of combinations of different degradation footprints in measured parameters. Hanachi et al. (2018) [18] emphasized that accurate diagnosis of engine faults through limited measurements has always posed a challenge. However, increasing the number of engine sensors will improve the precision of the diagnosis, but life cycle cost will be increased substantially [19]. The improvement of the diagnostic accuracy of gas turbines engines with limited measurement sets has attracted the attention of researchers in both academia and industry. Jasmani et al. (2011) [20] reported a measurement selection method for triple-shaft engine diagnostics that showed improved accuracy when compared with measurements on-site. However, the prediction error increased when there were more than three degraded components. Pinelli et al. (2012) [21] considered keeping some of the health parameters fixed by an a-priori optimized selection for engine diagnosis and used the concept of multiple operating points for addressing limited measurements on-site. Hanachi et al. (2014) [22] introduced a diagnostic technique for gas turbines, in which the degradation magnitudes are quantified by heat loss and power deficit indices, rather than the health index of each rotating component. Lu et al. (2016) [23] proposed an improved and extended Kalman filter to address the shortage of available measurements by the linear combination of the health parameters, but the diagnostic accuracy was affected by the transformation matrices. Mohammadi and Montazeri-Gh (2016) [24] developed a global optimization-based engine diagnostic method to overcome the lack of measurement instrumentation. Qingcai et al. (2016) [25] conducted a series of sensitivity analyses, in which they chose different degradation levels to quantify the measurement deviation of a triple-shaft engine. However, actual engine component degradation and ambient conditions could fall outside the range of the case studies examined. Besides, the estimation of the correct degradation level through real measurement deviation and chart of sensitivity analysis remains questionable. Sun et al. (2016) [26] proposed a GPA method to overcome the lack of measurement parameters by fusing information from other sources. Simon and Rinehart (2016) [19] suggested a sensor selection for aero-engines based on the Kalman filter and a maximum a posteriori estimator, but they assumed the faults occurred in isolation. Yang et al. (2018) [27] proposed multiple interacting models for fault detection and isolation. Then, they applied a generalized likelihood ratio approach for fault quantification. As the number of multiple models was limited, their scheme assumed that the failures did not occur simultaneously. In 2019, Yang et al. [28] developed a new multiple model-based engine fault diagnosis algorithm, but the assumption of multiple models remained. Despite the recent progress in engine diagnostics, the limited set of engine measurements is still one of the most significant challenges for fault diagnosis [17].

From a computation perspective, increasing the matrix dimensions for the iterative diagnostic algorithm may lead to the dimensionality problem [29]. It is worth emphasizing that the computation will increase exponentially under these conditions [30]. Daroogheh et al. (2017) [31] pointed out that the number of required samples increases exponentially for particle filters when the dimensionality of the health parameters increases. To date, studies have investigated the demand for improving the computation speed for engine diagnostics. Tsoutsanis et al. (2014) [32]

proposed an adaptive diagnostics method for detecting compressor degradation through map tuning based on a heuristic optimization technique. However, increasing the number of degraded components may lead to local and not globally optimal solutions. Ying et al. (2016) [16] conducted fault detection before fault diagnosis, which could reduce the dimension of the fault coefficient matrix. However, the scheme is not applicable when all components degrade simultaneously. Yang et al. (2018) [33] suggested that the computation burden could be reduced by the generalized expression of the Jacobian matrix, although the dimension of the matrix remained the same. Lu et al. (2018) [34] proposed a fusion unscented Kalman filter to reduce the computation time of fault diagnosis by improving the convergence speed. However, the diagnosis only considered efficiency degradation, and the flow capacity was excluded during fault diagnosis.

Overall, the above studies highlight the need for accurate diagnosis of engine degradation with a limited number of measurements and improved computational performance under the simultaneous deterioration of multiple components. In this study, a sequential diagnostic method for improving the precision and computation efficiency is proposed and applied to a triple-shaft industrial gas turbine with all five rotating components degraded simultaneously. The procedure of sequential diagnosis allows the partition of the diagnostic algorithm into several serial mechanisms to remove the smearing effect and reduce the matrix dimension in the iterative diagnostic algorithm. Furthermore, the problem of limited measurements is addressed by feeding multiple operating points into the diagnostic process. The novel contributions of this work are as follows:

1) A gas turbine engine model with object-oriented and modularized architecture has been developed in the Microsoft Visual Studio C# environment [35], which is validated against GasTurb. The model's architecture is suited to the sequential diagnostic algorithm, which is evaluated through a well-used diagnostic method.
2) The new method improves diagnostic accuracy by isolating the fault components and eliminating the smearing effect via sequential analysis.
3) The novel algorithm decreases the computation time by reducing both the matrix's dimensions in the iteration algorithm and the number of calls to engine sub-models (compressor model, burner model, turbine model, etc.).
4) The proposed scheme can ensure the required diagnostic accuracy, under a limited number of measurements, by multiple operating point analysis. Reducing the number of measuring sensors can potentially bring economic benefits to the engine operator and decrease sensor related problems.

5) The negative impact of measurement noise on fault diagnosis accuracy is addressed by an averaging filter for data filtration to demonstrate the suitability of the method for real-world applications.

The remainder of this paper is organized as follows. Section 2 is concerned with the methodology used for this study. Section 3 demonstrates the validation of the developed engine model using commercial software. Section 4 analyses the results of the fault diagnosis. The final section presents the conclusions of the research.

2. Methodology

2.1 Engine Performance Model

The triple-shaft industrial gas turbine engine used in this study (Fig. 1) is similar to the Rolls-Royce RB211-24G operated at the China Petroleum Pipeline Langfang compressor group [36]. The power output is selected as the control variable in this study, but this could be any other control parameter, such as rotation speed, fuel flow rate, etc. The existing measurement parameters on-site are shown in Table 1 [36]. It is worth noting that the measurements at HPT outlet are not available due to the high gas temperature.

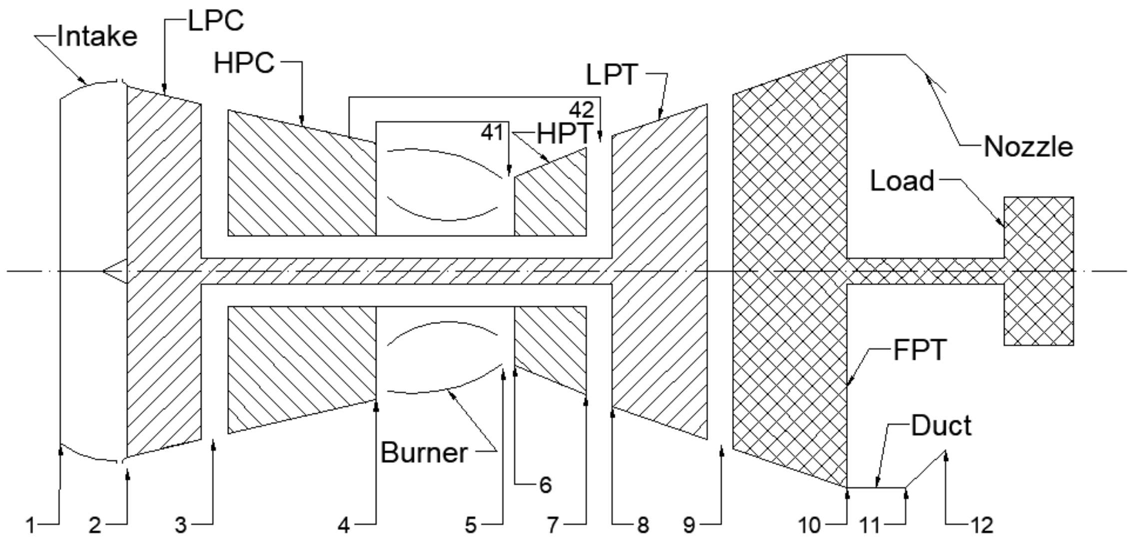

Fig. 1 Schematic layout of the triple-shaft engine configuration, with station numbering.

In general, the performance of a gas turbine engine is a function of its components' performance [37]. Hence, the degradation factor (X) of each component is defined as the ratio of the degraded state over the healthy state of each characteristic parameter (CP), as Eq. **(1)** [38]. X equals unity means a healthy/clean state.

$$X = \frac{CP_{ac}}{CP_{ideal}} \quad \textbf{(1)}$$

where the subscript "ac" represents the actual characteristic parameter of component, while "ideal" represents the healthy/clean characteristic parameter obtained from the component map.

Table 1 Available engine gas path measurements on-site [36]**.**

No	Available Measurement Parameters	Symbol
1	Ambient pressure	P_1
2	Ambient temperature	T_1
3	Ambient relative humidity	RH_1
4	Free power turbine shaft rotational speed	N_{FPT}
5	Free power turbine output	TW_{FPT}
6	Low-pressure compressor (*LPC*) exit pressure	P_3
7	*LPC* exit temperature	T_3
8	High-pressure compressor (*HPC*) exit pressure	P_4
9	*HPC* exit temperature	T_4
10	Low-pressure turbine (*LPT*) exit pressure	P_9
11	*LPT* exit temperature	T_9
12	Free power turbine (*FPT*) exit pressure	P_{10}
13	*FPT* exit temperature	T_{10}
14	*LP* shaft rotational speed	N_{LP}
15	*HP* shaft rotational speed	N_{HP}
16	Burner fuel flow rate	W_{Fuel}

The engine model is crucial for model-based diagnostics in order to assess the performance state of a gas turbine engine [39]. A thermodynamic model of the engine has been developed in Microsoft Visual Studio C#. A detailed description of the model and its governing equations are presented in Appendix B. The balancing process for off-design simulation of the triple-shaft industrial gas turbine is based on [40]. The assumptions that have been made for the developed model are as follows:

1) It is assumed that the compressors are of fixed geometry.
2) Pressure losses in the burner and duct models are accounted for by assuming that the losses are proportional to the inlet conditions.
3) Isentropic expansion is assumed in the model of the exhaust nozzle.

4) The mixture model includes two inlet flows, namely the main flow and the cooling flow. The mixture's total outlet pressure is assumed to be equal to the absolute inlet pressure of the main flow.

The effect of relative humidity is considered in the developed engine model. The gas property of the engine model is generated via the NASA CEA program [41], where both fuel-air ratio (FAR) and water-to-air-ratio (WAR) are considered to define the mixtures. When two of the gas properties and mixtures are defined/known, the remaining gas properties can be calculated. For example, when the temperature (T), pressure (P), FAR, and WAR are known, the enthalpy (H), entropy (S), and density (ρ) etc. could be obtained using Eq. **(2)**.

$$[H, S, \rho, \ldots] = GasProp_{[T,P]}(T, P, FAR, WAR) \tag{2}$$

It is worth mentioning that the gas turbine of interest does not include water injection at any station of the engine. Hence, the WAR is a constant throughout the engine and varies only with a change in ambient conditions.

2.2 Conventional Diagnostic Method

The scheme of the conventional model-based diagnostic system is shown in Fig. 2 [42–44]. Irrespective of the number of degradation components considered, the diagnostic system should run the performance simulation of the entire engine model (call all engine sub models each time). In such a condition, the algorithm will consume significant computational power and may suffer from smearing. The nonlinear gas path analysis (NLGPA) combined with multiple operating point analysis has been widely used for model-based fault diagnosis, as shown in Eq. **(3)** [45]:

$$Z_{i \cdot m} = f(X_l) \tag{3}$$

where $f(\cdot)$ is the nonlinear vector-valued function of gas turbine performance, Z denotes the measurement parameters, $\forall\, i = 1, \ldots, n$, $\forall\, m = 1, \ldots, M$, and $\forall\, l = 1, \ldots, L$ where "n", "M", and "L" denote the number of operating points, the number of measurements, and the number of degradation factors, respectively. The NLGPA solver could be of any type, but the most popular for gas turbine engines are: Newton-Raphson [46], Kalman filter [47], Particle filter [31], and Genetic Algorithms [25].

Remark 1. *It is worth noting that the first five measurements in Table 1 are used to establish the engine operating condition for conventional model-based diagnostics, and as such, the gas path measurements for fault diagnosis in Eq.* ***(3)*** *are the remaining 11 parameters.*

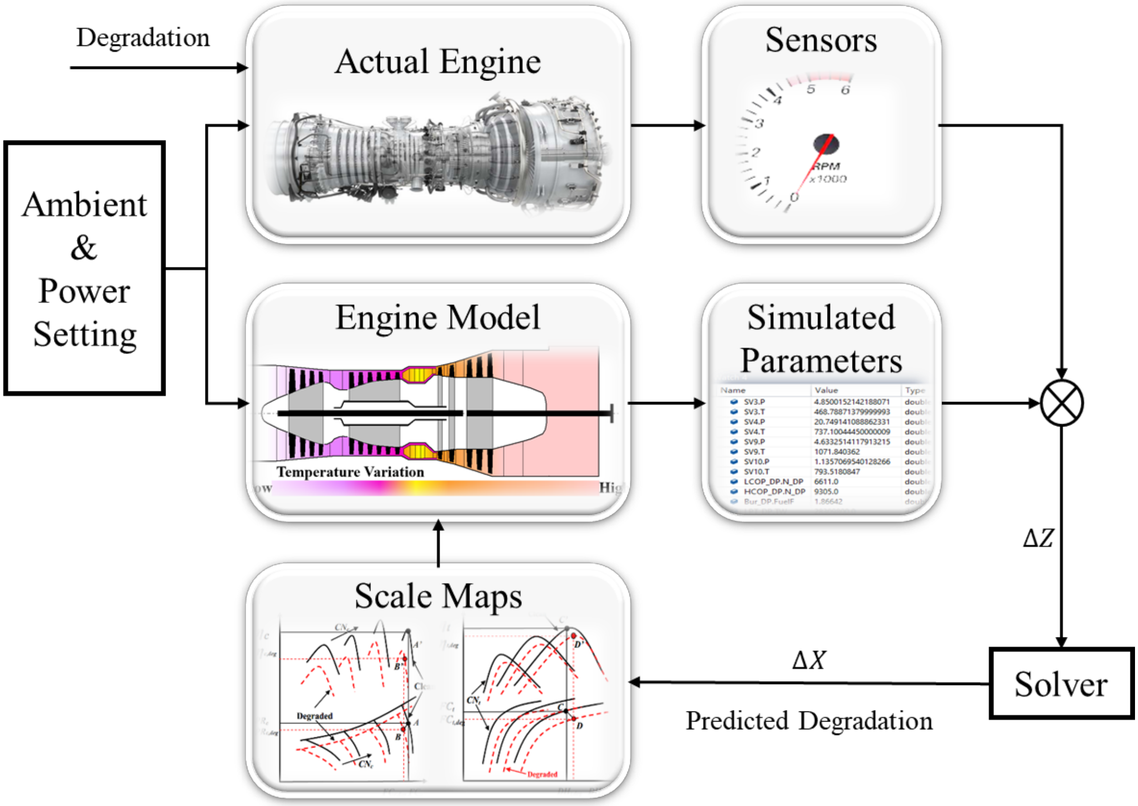

Fig. 2 Schematic layout of the conventional gas path analysis process [42–44]**.**

The component health parameters considered in this study are summarized in Table 2.

Table 2 Degradation factors of the individual rotating component.

Component	**Symbols**		**Component Health Parameters**
LPC	X_{LPC}	$X_{LPC,E}$	LPC efficiency degradation factor
		$X_{LPC,F}$	LPC flow capacity degradation factor
HPC	X_{HPC}	$X_{HPC,E}$	HPC efficiency degradation factor
		$X_{HPC,F}$	HPC flow capacity degradation factor
HPT	X_{HPT}	$X_{HPT,E}$	HPT efficiency degradation factor
		$X_{HPT,F}$	HPT flow capacity degradation factor
LPT	X_{LPT}	$X_{LPT,E}$	LPT efficiency degradation factor
		$X_{LPT,F}$	LPT flow capacity degradation factor
FPT	X_{FPT}	$X_{FPT,E}$	FPT efficiency degradation factor
		$X_{FPT,F}$	FPT flow capacity degradation factor

The root mean square error of the measurement parameters ($RMSE_{Mea}$) is calculated using Eq. **(4)** to check the convergence of NLGPA iterations. When the maximum allowed iteration step (21 in this study) is achieved, then the calculation will stop without convergence. In this situation, the $RMSE_{Mea}$ is larger than the threshold (1E-5).

$$RMSE_{Mea} = \sqrt{\left[\sum_{i=1}^{n\cdot M}\left(\frac{Z_{i,ac} - Z_{i,pd}}{Z_{i,ac}}\right)^2\right]/(n\cdot M)} \tag{4}$$

where the subscript "pd" and "ac" referred to the predicted and actual values, respectively.

The root mean square error of the degradation factor ($RMSE_X$) is defined by Eq. **(5)** to evaluate the diagnosis of the degradation factor.

$$RMSE_X = \sqrt{\left[\sum_{i=1}^{L}\left(\frac{X_{i,ac} - X_{i,pd}}{X_{i,ac}}\right)^2\right]/L} \tag{5}$$

Remark 2. *It should be noted that the actual degradation is not available, and $RMSE_X$ is used in this study only to assess the performance of the developed method.*

The relative error (λ_i) is defined by Eq. **(6)** and represents the percentage ratio of the absolute difference between the predicted and actual/implanted degradation factors, to the actual degradation.

$$\lambda_i = \frac{\left|X_{i,ac} - X_{i,pd}\right|}{X_{i,ac}} \times 100\% \tag{6}$$

2.3 Novel Sequential Diagnostic Method

2.3.1 Novel Sequential Diagnostic Method with All Available Measurements

The architecture of sequential diagnosis is shown in Fig. 3, where the dotted lines and the solid lines in the graph indicate the flow of information of target parameters and to-be adapted parameters, respectively. The diagnostic scheme partitions the engine diagnosis into four sequential steps for the triple-shaft engine of interest. The FPT diagnostic is carried out first. The diagnosis then resumes in the LPC, then in the HPC, and finally, the HPT and LPT conclude the diagnosis. The dotted boxes in Fig.3 indicate the available gas path measurements for each step.

The subsequent sections describe the sequential procedure in more detail.

➢ *Step 1: Free Power Turbine Diagnostics*

Step 1 in this process involves the tuning of the FPT map, through the scaling factors X_{FPT} ($X_{FPT,E}$, $X_{FPT,F}$), which will eventually enable the model to match the available measurements at outlet temperature (T_{10}) and turbine power output (TW_{FPT}). This step involves only the turbine model during iteration, which can potentially save a lot of computation time.

➢ *Step 2: Low-Pressure Compressor Diagnostics*

Similar to the previous step, the X_{LPC} ($X_{LPC,E}$, $X_{LPC,F}$) is estimated through an iterative process to scale the compressor map according to the compressor model based on the LPC outlet temperature (T_3) and W_2.

➢ *Step 3: High-Pressure Compressor Diagnostics*

At the HPC stage, the X_{HPC} ($X_{HPC,E}$, $X_{HPC,F}$) is also tuned to scale the compressor map for the simulation of the compressor model. The two measurements to be satisfied are T_4 and W_3, with the latter having been calculated from Step 2. By iteration, the corrected X_{HPC} can be determined, and the HPC diagnostic needs to utilize only the compressor model during iteration.

➢ *Step 4: High-pressure and Low-pressure Turbine Diagnostics*

The pressure ratio of HPT (PR_{HPT}), X_{HPT} and X_{LPT} are the iteration variables for Step 4, where X_{HPT} ($X_{HPT,E}$, $X_{HPT,F}$) and X_{LPT} ($X_{LPT,E}$, $X_{LPT,F}$) are tuned to scale the HPT and LPT maps respectively during iteration. The work compatibility of the *HP* and *LP* shafts, and LPT outlet temperature (T_9) are available as convergence criteria to tune the iteration variables.

Remark 3. *There are three convergence criteria for a single operating point of the gas turbine in Step 4. Hence, the number of convergence criteria is (*$\mathrm{n} \times 3$*) for n operating points. The total iteration variables are (*$4 + \mathrm{n}$*) for n different operating points, where the number "4" denotes the four degradation factors for* HPT *and* LPT*, and "n" denotes the required number of* PR_{HPT} *for each operating point of the gas turbine. The* n *is assigned to be three, which is the minimum number of operating points to satisfy the requirement that the number of convergence criteria (nine) should be more than the iteration variables (seven). A more detailed description of the iterative matrix computation for the proposed diagnostic method is provided in Appendix A.*

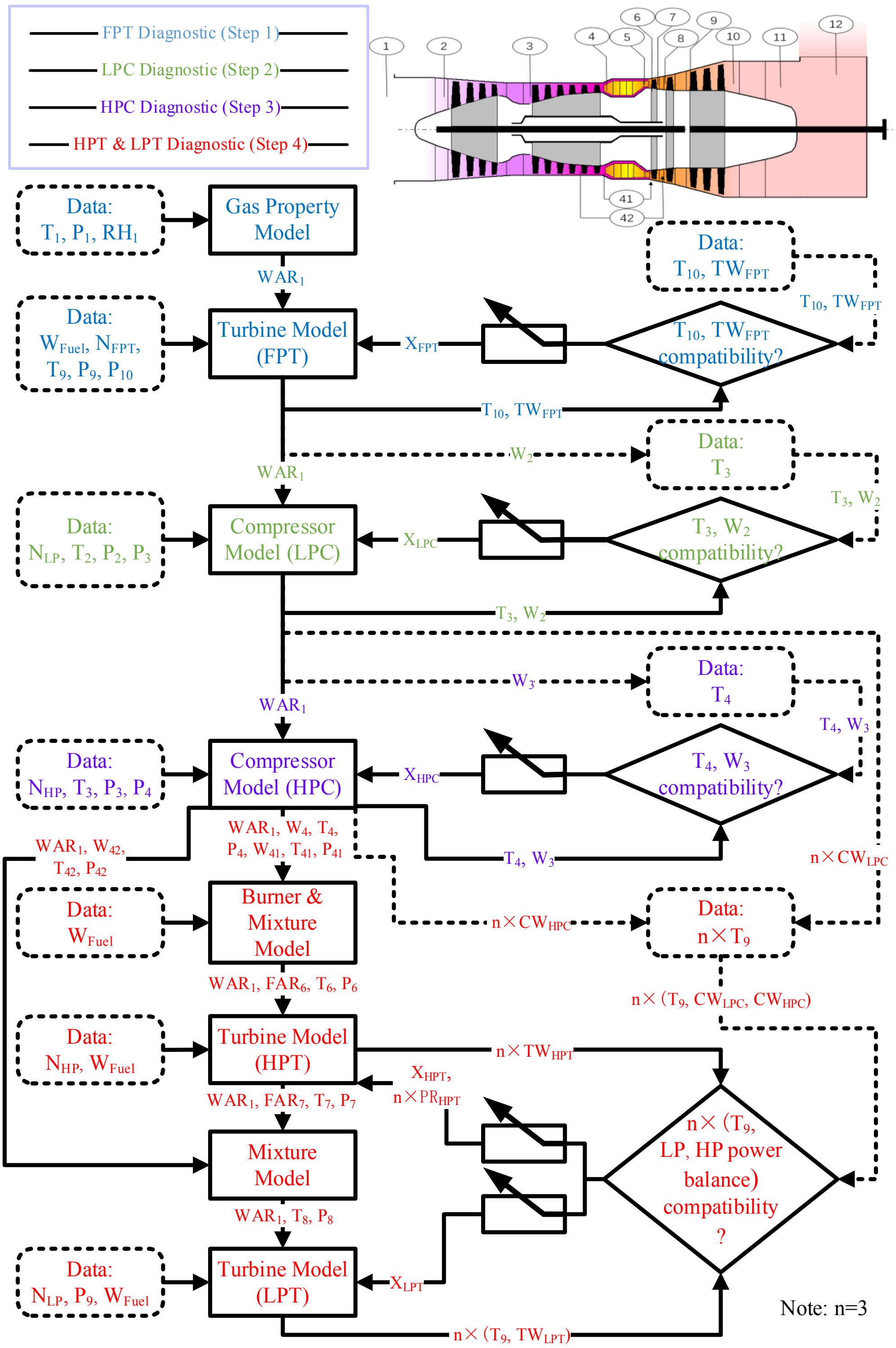

Fig. 3 Sequential diagnostic scheme of gas turbine with all available measurements.

2.3.2 Novel Sequential Diagnostic Method with Reduced Number of Measurements

Shaft power of aero engines is a parameter which is more challenging to obtain accurately in comparison to land-based or marine engines, where it can be found through engine load. Hence, it is necessary to test the FPT diagnostic without the measurement of power output (TW_{FPT}). Additionally, the gas path measurements at the LPC outlet (T_3 and P_3) will be assumed unavailable.

Now, the sequential diagnostic divides the entire triple-shaft engine into three diagnostic steps: FPT diagnostics, LPC and HPC diagnostics, and HPT and LPT diagnostics. The diagnostic scheme with reduced measurements is shown in Fig. 4, where the dotted lines and solid lines indicate the flow of information of target parameters and to-be aligned parameters, respectively. The FPT diagnostic step is now modified, in comparison to the previous approach, in order to assess the suitability of this method for aero engine applications. Meanwhile, HPC and LPC diagnostics (Step 2-3) are also modified to reduce the number of gas path measurements further. For HPT and LPT, the diagnosis is the same as presented in Fig. 3, and the calculation process will not be further discussed here. The dotted boxes indicate the available gas path measurements for each step.

➢ *Step 1: Free Power Turbine Diagnostics*

The X_{FPT} ($X_{FPT,E}$, $X_{FPT,F}$) is estimated through an iterative process to scale the component map for the turbine model. There is only one targeted parameter available for a single operating point (*n*) of the gas turbine, and that is the FPT outlet temperature (T_{10}).

➢ *Step 2: High-pressure and Low-pressure Compressors Diagnostics*

In the second step of this process, the pressure ratio of LPC (PR_{LPC}), X_{LPC} and X_{HPC} are utilized to satisfy three measurement parameters, namely W_2, W_3 and T_4. Once again X_{LPC} ($X_{LPC,E}$, $X_{LPC,F}$) and X_{HPC} ($X_{HPC,E}$, $X_{HPC,F}$) are tuned to scale the LPC and HPC maps, respectively, during iteration.

Remark 4. *The number of operating points, n, is three for every step, which is the least number of operating points capable of satisfying the convergence requirements.*

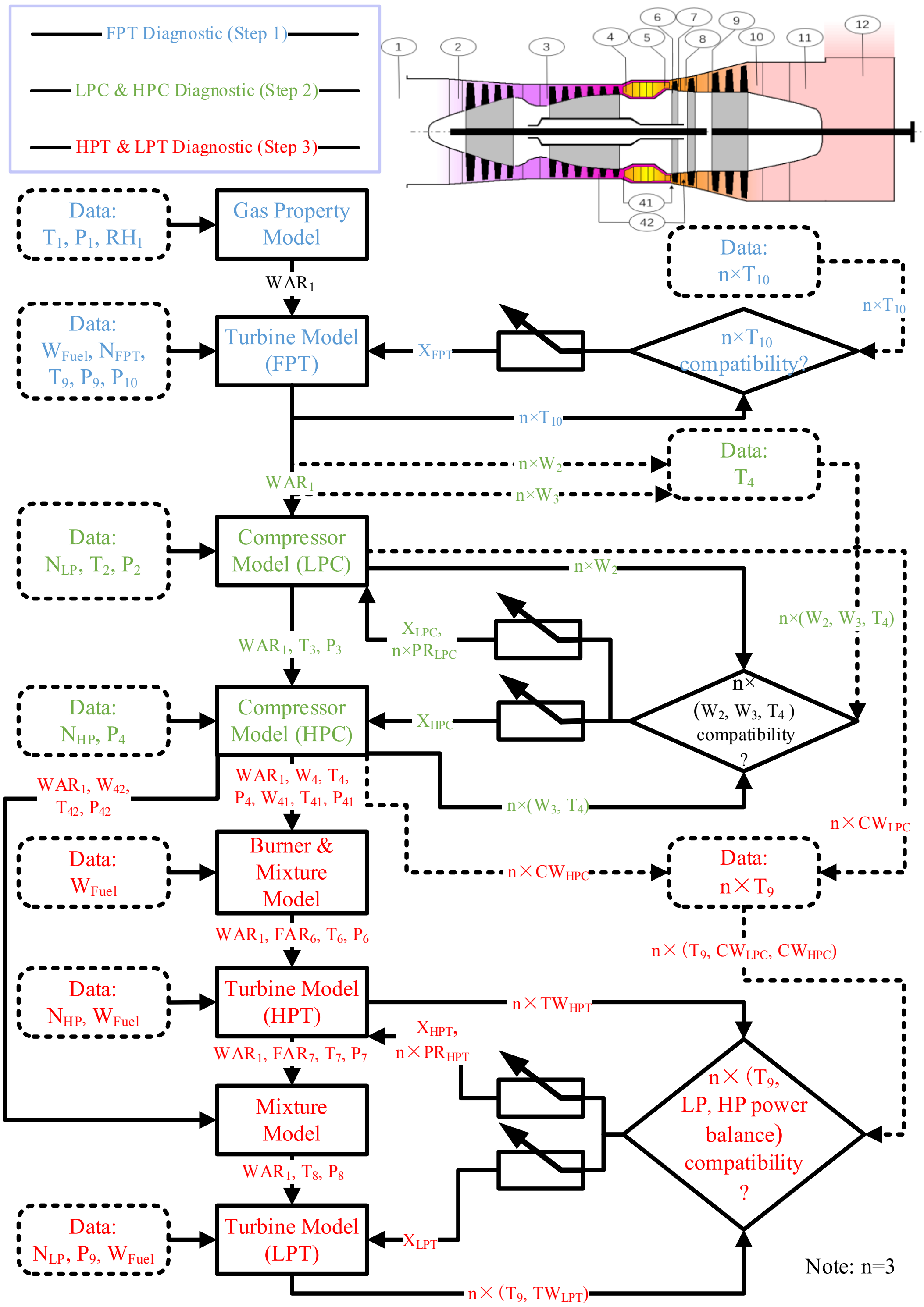

Fig. 4 Sequential diagnostic scheme of gas turbine with reduced measurements.

2.4 Method Overview

Essentially, the proposed sequential diagnostic method partitions the engine model into several sequential steps to reduce the dimensions of the matrices and the number of calls to each engine component model during diagnosis. A detailed analysis of the computational burden of both methods is given in Appendix A. Another key feature of the sequential diagnosis method is its capability of eliminating the smearing effect by isolating components with the aid of multiple operating point analysis. The sequential diagnostic method is tested with reduced engine gas path measurements, which will not only reduce the cost to engine operators but also reduce flow disturbances caused by the installation of sensors.

3. Engine Model Validation

The developed engine model has been validated against the commercial gas turbine software GasTurb [44]. The engine operating conditions at the design point are shown in Table 3. The design point simulation algorithm is validated first, and the relative errors are shown in Table 4, which indicates that the maximum relative error is less than 0.31%. It follows that the developed engine performance model is satisfactory at the design point.

Table 3 Engine specification.

Parameters	Symbols	Unit	Value
Ambient Pressure	P_1	atm	1.000
Ambient Temperature	T_1	Kelvin	288.15
Ambient Relative Humidity	RH_1	%	60.00
Inlet Air Flow Rate	W_1	kg/s	83.40
LPC Rotational Speed	N_{LP}	rpm	6611
HPC Rotational Speed	N_{HP}	rpm	9305
FPT Rotational Speed	N_{FPT}	rpm	4800
FPT Power Output	TW_{FPT}	MW	28.31

The power output of the gas turbine varies with respect to the actual load demand. Hence, it is essential to check whether the developed algorithm can provide satisfactory results at steady-state off-design conditions. The same component maps are used for both the GasTurb and the developed engine model for off-design validation. Four measured parameters are shown in Fig. 5, where a comparison is made between the GasTurb and the developed model. Specifically, the HPC outlet temperature (T_4), FPT inlet pressure (P_9), LPC rotational speed (N_{LP}), and fuel flow rate (W_{Fuel}) are considered at different power settings, varying from 65% to 100% with a step of 5%.

Table 4 Engine model validation at design point [44]**.**

Parameters	Units	GasTurb[44]	Developed Model	Relative Error [%]
P_3	atm	4.850	4.850	0.000
T_3	Kelvin	468.70	468.79	0.019
P_4	atm	20.749	20.749	0.000
T_4	Kelvin	737.11	737.10	0.001
P_5	atm	20.127	20.126	0.005
T_5	Kelvin	1494.00	1494.20	0.013
P_6	atm	20.127	20.126	0.005
T_6	Kelvin	1459.49	1459.77	0.019
P_7	atm	8.605	8.588	0.198
T_7	Kelvin	1233.58	1234.41	0.067
P_8	atm	8.605	8.588	0.198
T_8	Kelvin	1216.03	1216.84	0.067
P_9	atm	4.647	4.633	0.301
T_9	Kelvin	1071.23	1071.84	0.057
P_{10}	atm	1.139	1.136	0.263
T_{10}	Kelvin	793.26	793.52	0.033
W_{Fuel}	kg/s	1.866	1.867	0.006

The results demonstrate that the developed model is capable of predicting the gas turbine performance at different operating conditions with a high degree of precision relative to GasTurb. The maximum relative error increases slightly as the power decreases, which is reasonable since we are moving further away from the design point, and the maximum relative error for all parameters listed in Table 4 is less than 0.71% at 65% power setting for W_{Fuel}, as shown in Fig. 5. Another cause for the increasing error may be attributed to the different methods of reading the component map in the calculation procedure. Although the errors increase at lower power settings, the developed model retains a good agreement with GasTurb. Therefore, the developed engine model will be implemented to quantify the level of degradation for both conventional and newly proposed staged diagnostic methods.

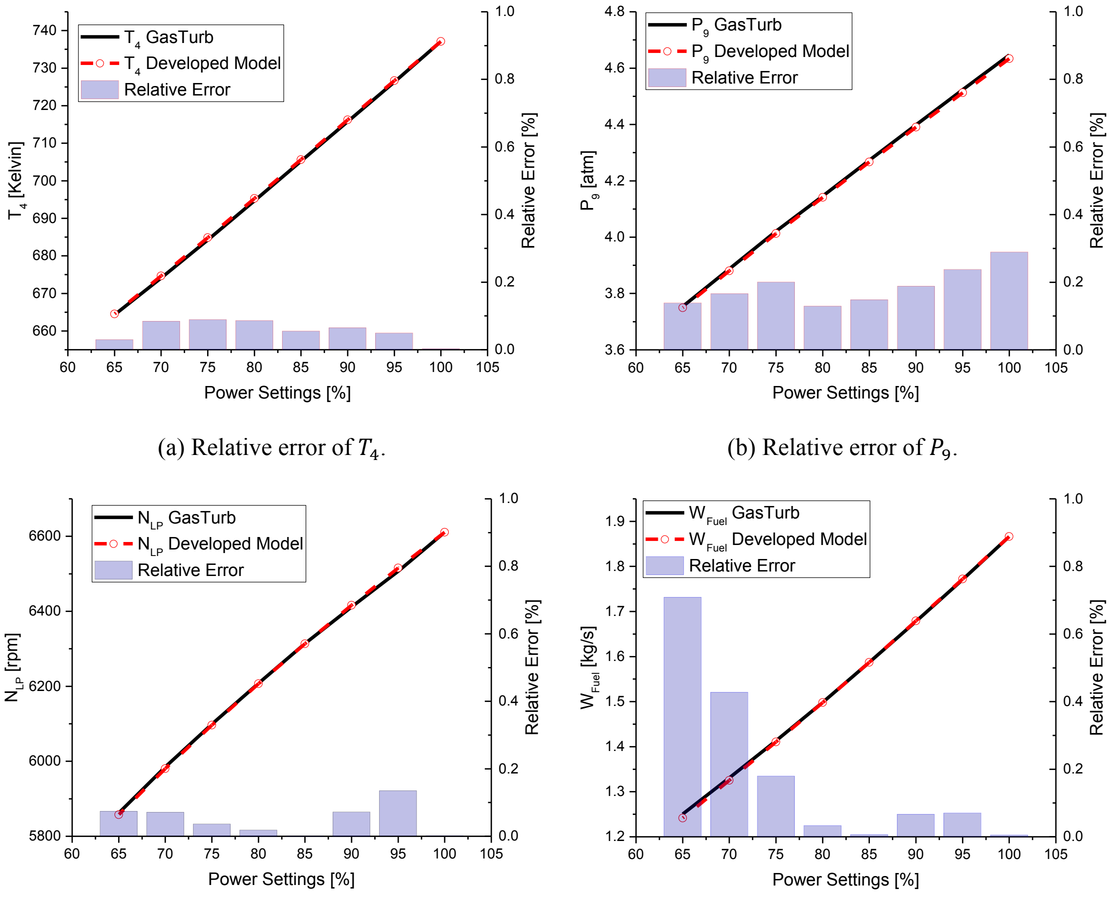

(a) Relative error of T_4.

(b) Relative error of P_9.

(c) Relative error of N_{LP}.

(d) Relative error of W_{Fuel}.

Fig. 5 Engine model validation at off-design points [44].

4. Application and Analysis

4.1 Case Study Description

Four case studies are conducted to assess the accuracy and the computational performance of the proposed diagnostic method. Moreover, the developed method will be compared with the conventional NLGPA method [45]. The case studies are as follows:

Case 1: The objective of this case study is to test the conventional diagnostic method NLGPA [45] in order to establish a benchmark against which comparisons will be made.

Case 2: The objective of this case study is to test the proposed sequential method in terms of diagnostic accuracy and computational speed.

Case 3: This case study is based on the sequential method, similar to Case 2, with the only difference being the reduced number of available engine measurements. The goal is to assess the suitability of the proposed method for application to gas turbine engines that have relatively fewer measurement sensors.

Case 4: The objective of this case study is to test the effectiveness of the proposed method in providing an accurate diagnosis in the presence of measurement noise.

With the accumulation of running time, all components will degrade. In this paper, the typical degradation implanted into all rotating components, to represent compressor fouling and turbine erosion, of the engine model is shown in Table 5 [46]. The typical degradation is injected into the reference engine state using Eq. **(1)** to obtain component characteristics under deterioration. The degradation factor, X, consists of isentropic efficiency and flow capacity.

Table 5 Typical degradation level for engine rotating components [46]**.**

Component	Degradation Type	Parameter	Degradation Level [%]
LPC	Fouling	$X_{LPC,E}$	-1.0
		$X_{LPC,F}$	-4.0
HPC	Fouling	$X_{HPC,E}$	-1.0
		$X_{HPC,F}$	-4.0
HPT	Erosion	$X_{HPT,E}$	-1.0
		$X_{HPT,F}$	+2.0
LPT	Erosion	$X_{LPT,E}$	-1.0
		$X_{LPT,F}$	+2.0
FPT	Erosion	$X_{FPT,E}$	-1.0
		$X_{FPT,F}$	+2.0

The case studies have been conducted in a PC with Intel® Core™ i7, 2.9 GHz, and 16 GB RAM. The software environment in which the model is developed in Visual Studio C# and the iterative algorithm used in all case studies is the Newton-Raphson [48]. The above features remain constant for all case studies in order to demonstrate and illustrate the advancement of the sequential diagnostic method.

4.2 Case 1: Conventional Diagnostic

Case 1 involves five simultaneously degraded components, with up to three operating points (n), and it follows the process is as schematically represented in Fig. 2. In the first diagnostic attempt we use a single operating point in the NLGPA method [45], and the calculation converges in 7 steps, shown in Fig. 6 (a), with the $RMSE_{Mea}$ less than 1E-5, see Table 6. However, when checking the $RMSE_X$, it becomes evident that the predicted degradation factor is not identical to the implanted fault. This highlights the presence of the smearing effect, where a different combination of degradation factors could match the engine measurements.

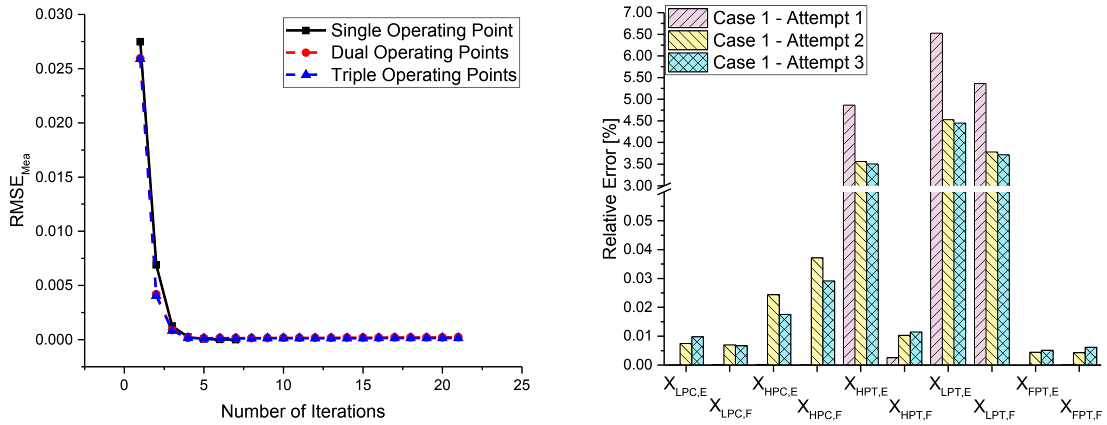

(a) Convergence of diagnosis. (b) Relative diagnostic error.

Fig. 6 Convergence performance and relative diagnostic error for Case 1.

Table 6 Diagnostic results of Case 1.

Items	Symbols	Units	Attempt 1	Attempt 2	Attempt 3
Computation Time	CT	Second	22.659	129.682	197.368
Measurement Error	$RMSE_{Mea}$	-	4.3E-6	2.1E-4	1.6E-4
Degradation Factor Error	$RMSE_X$	-	2.9E-2	1.5E-2	1.2E-2
Operating Point	n	-	1	2	3
No. of Iteration Steps	NIS	-	7	21	21
No. of total calls to engine sub-models	NO_{Model}	-	94644	566775	841797

In the second and third attempts, we consider two and three operating points, respectively. In both attempts the $RMSE_{Mea}$ condition is not satisfied, and the iterations terminate at the maximum allowed step, as shown in Table 6. Although the $RMSE_X$ decreases as the operating points increase, it is still noticeable (Table 6). The results reveal that the multiple operating point analysis did not eliminate the smearing effect in these two attempts. The computation time increases significantly when increasing the operating points from one to two to three; 22.659, 129.682, and 197.368 seconds, respectively. The comparison between implanted and predicted degradation factors is shown in Fig. 6 (b), where all three cases could not achieve high diagnostic accuracy. Table 6 illustrates the computation burden of three attempts by conventional diagnosis methods with an increasing number of operating points.

4.3 Case 2: Sequential Diagnostic with All Measurements

In Case 2, the sequential diagnostic method is employed, where the diagnosis is partitioned into four steps, as shown in Fig. 3. Convergence processes for these four sequential steps are demonstrated in Fig. 7 (a). It is clear from Fig. 7 (b) that the sequential diagnostic has the capability to estimate the degradation factor with greater accuracy than the conventional diagnostic method (Case 1). It is worth noting that the last step of the proposed sequential method requires three operating points to determine the degradation factor and eliminate the smearing effect, something that the conventional diagnostic could not do.

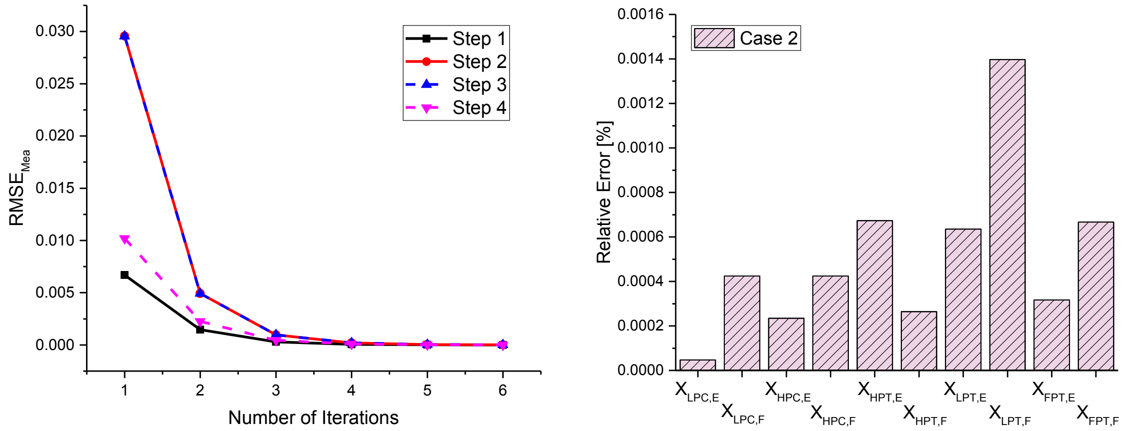

(a) Convergence of diagnosis. (b) Relative diagnostic error.

Fig. 7 Convergence performance and relative diagnostic error for Case 2.

The four sequential diagnostic steps converge in 0.014, 0.011, 0.013, and 0.032 seconds, respectively, as shown in Table 7. The proposed diagnostic process converges in 0.070 seconds (sum of all four sequential steps) for the simultaneous deterioration of all five rotational components. The reason for this fast convergence lies in the reduction of matrix dimensions in the iteration algorithm and the reduced total number of calls to the engine sub-models (Table 7). Comparing the total number of calls to engine sub-models in Table 6 and Table 7 illustrates that the sequential diagnostic requires less computation than the conventional diagnosis. Moreover, it is evident that the novel sequential diagnostic process is also superior to the traditional diagnostic method in terms of accuracy, as shown in Fig. 6 (b) and Fig. 7 (b). It should be pointed out that the level of diagnostic accuracy achieved by this method remains the same, even for smaller levels of engine component deterioration.

Table 7 Diagnostic results of Case 2.

Items	Symbols	Units	Step 1	Step 2	Step 3	Step 4
Computation Time	CT	Second	0.014	0.011	0.013	0.032
Measurement Error	$RMSE_{Mea}$	-	2.4E-6	7.6E-6	7.6E-6	3.6E-6
Degradation Factor Error	$RMSE_X$	-	5.2E-6	3.0E-6	3.4E-6	5.7E-6
Operating Point	n	-	1	1	1	3
No. of Iteration Steps	NIS	-	6	6	6	6
No. of total calls to engine sub-models	NO_{Model}	-	18	18	18	438

4.4 Case 3: Sequential Diagnostic with Reduced Number of Measurements

For aero engines, the indirect measurement of turbine power output may not be possible or lead to poor precision. Hence, it is worth testing the sequential diagnostic method, without the power output measurement of the last turbine, in order to assess the suitability of the proposed approach for aero engine applications. It follows that the FPT fault diagnosis step, shown in Fig. 3, will be adapted so that it does not require the shaft power of the FPT, shown in Fig. 4.

As can be seen in Table 1, there is no measurement available at the outlet of the HPT due to the high gas temperature. Moreover, the sequential diagnosis with multiple operating points can estimate the correct degradation factor for HPT and LPT in Case 2. Hence, it is worth testing the possibility of eliminating the measurements T_3 and P_3 at the LPC outlet.

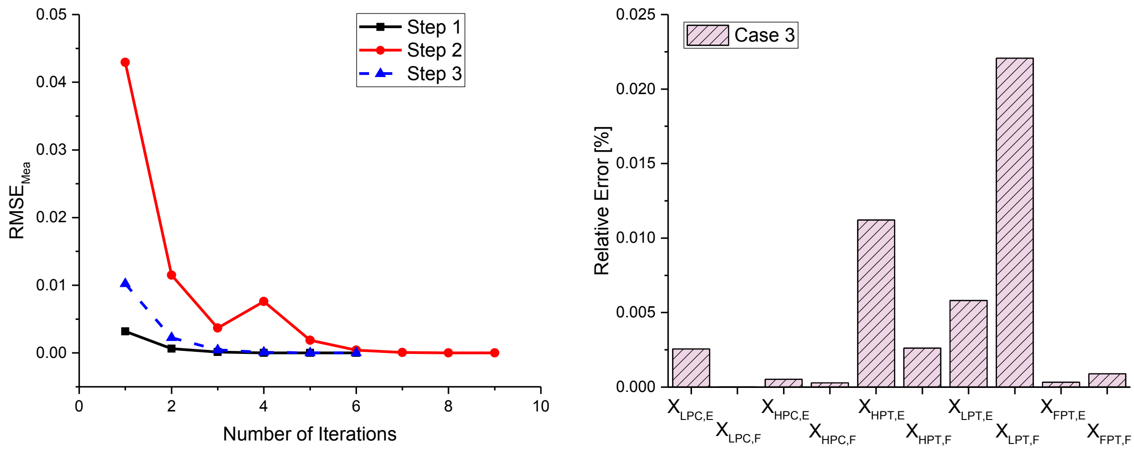

(a) Convergence of diagnosis. (b) Relative diagnostic error.

Fig. 8 Convergence performance and relative diagnostic error for Case 3.

In Case 3, the NLGPA includes three sequential steps, as shown in Fig. 4. The convergence performance of the three steps is shown in Fig. 8 (a). It is clear from Fig. 8 (b) that the sequential diagnostic with reduced number of measurements could still predict the degradation factor with excellent precision.

The degradation diagnosis for the three steps converges in 0.012, 0.065, and 0.031 seconds, respectively, as shown in Table 8. In total, the sequential diagnostic takes 0.108 seconds for the simultaneous deterioration of all five rotational components. Although the computation time has increased by 54.29% when compared with Case 2 (0.070 seconds) due to increased matrix dimensions and computation burden attributed to the multiple operating point analysis (Table 8), the measurement of power output and sensors at LPC exit can be removed in this situation. It is noted that all three steps of the proposed sequential method require three operating points to determine the degradation factor and eliminate the smearing effect under the reduced measurement condition.

Table 8 Diagnostic results of Case 3.

Items	Symbols	Units	Step 1	Step 2	Step 3
Computation Time	CT	Second	0.012	0.065	0.031
Measurement Error	$RMSE_{Mea}$	-	1.0E-6	3.7E-6	3.6E-6
Degradation Factor Error	$RMSE_X$	-	5.5E-6	8.8E-6	8.5E-5
Operating point	n	-	3	3	3
No. of Iteration Steps	NIS	-	6	9	6
No. of total calls to engine sub-models	NO_{Model}	-	54	432	438

Comparison of the total number of calls to the engine sub-models as shown in Table 6 and Table 8, highlights that sequential diagnosis with a reduced number of measurements requires less computation than the conventional method [45]. Additionally, it is clear that the novel sequential diagnosis with reduced number of measurements still has a precision advantage over the traditional diagnostic method [45], as shown in Fig. 6 (b) and Fig. 8 (b). Furthermore, the $RMSE_X$ of the HPT and LPT diagnoses in Case 3 is increased by an order of magnitude in comparison with Case 2. Nevertheless, the $RMSE_X$ is still quite small and less than 1E-4. Despite a slight sacrifice in computation efficiency and diagnostic precision, reducing the number of sensors can reduce both the initial and operating cost of the gas turbine, but a compromise is always necessary between diagnostic accuracy and number of sensors installed.

The relative error of 10 degradation factors defined in Eq. **(6)** for Cases 1-3 are summarized in Fig. 9 in order to demonstrate the merits of the proposed sequential diagnosis. It is clear that the diagnostic precision of the proposed method is far more accurate than the conventional method [45]. The computation time, the maximum relative error of each case and the number of required sensors for Cases 1-3 are summarized in Table 9. There is a significant improvement when comparing the novel sequential and conventional methods in both diagnostic precision and computation speed. In Case 2, the maximum relative error is 1.4E-3 %, which is substantially smaller than that of the traditional method, since the sequential diagnostic method can resolve the smearing effect. The calculation speed of the method is over 300 times faster than the conventional method, and this is attributed to the reduction of the matrix's dimensions in the iterative diagnostic algorithm. In Case 3, the method demonstrates a maximum relative error of 2.2E-2 %, and the computation time of the proposed approach is more than 200 times faster than the traditional method.

Table 9 Comparison between three diagnostics cases.

Items	Symbols	Units	Case 1 Attempt 1	Case 1 Attempt 2	Case 1 Attempt 3	Case 2	Case 3
Computation Time	CT	Second	22.659	129.682	197.368	0.070	0.108
Max Relative Error	λ_{max}	%	6.52	4.53	4.45	1.4E-3	2.2E-2
No. of Sensors Required	NO_S	-	16	16	16	16	13

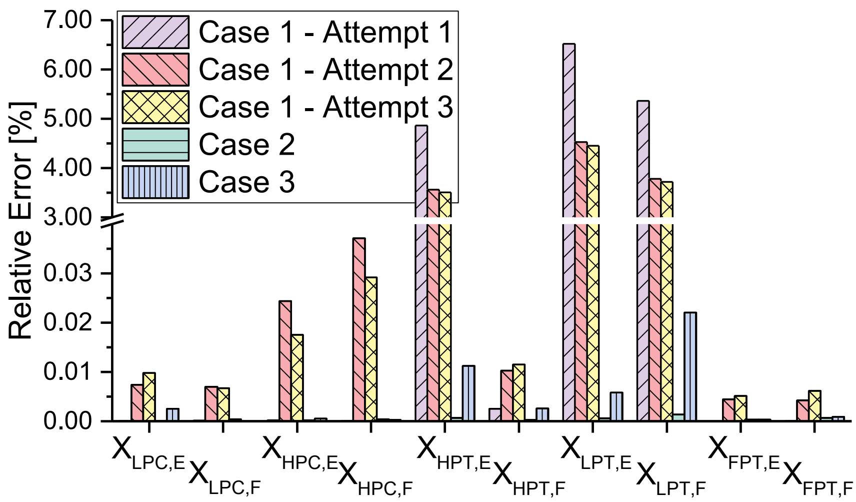

Fig. 9 Comparison of relative diagnostic error for three diagnostic cases.

4.5 Case 4: Effect of the Measurement Noise

To analyze the influence of noise on diagnostic accuracy, measurement noise generated via the engine thermodynamic model is imposed on the measured values. We have assumed that the noise is subject to a Gaussian distribution with zero mean and standard deviation one, and the maximum deviation is shown in Table 10 [49,50]. We assume that the engine measurements are recorded every 15 seconds, and for 5 minutes of steady-state operation, this means that there are 20 operating points available. Then, 20 sets of measurements with random noise added are generated for FPT fault diagnosis (Step 1) in Case 2. Two examples of such noisy measurements, namely N_{FPT} and T_9, are shown in Fig. 10. The 21st point is the post-filtered value of the measurement obtained from the previous 20 noisy data by an averaging filter [51], which is an averaging process of each measurement. The 22nd point represents the actual value of measurement, with no noise added. The preprocessed measurements (21st point) are used in Case 4, which is essentially a repetition of FPT fault diagnosis (Step 1) in Case 2.

Table 10 Maximum measurement noise [49,50]**.**

Measurement	Range	Typical Error
Pressure [atm]	0.204-3.06	0.50%
	0.544-31.30	0.5% or 0.125 atm whichever is greater
Temperature [°C]	-65-290	± 3.3
	290-1000	$\pm\sqrt{2.5^2 + (0.0075 \times T)^2}$
	1000-1300	$\pm\sqrt{3.5^2 + (0.0075 \times T)^2}$
Shaft Power	-	0.10%
Rotational Speed	-	0.10%
Relative Humidity [%]	-	0.10%
Fuel Flow [kg/h]	Up to 5450	63.4
	Up to 12260	142.7

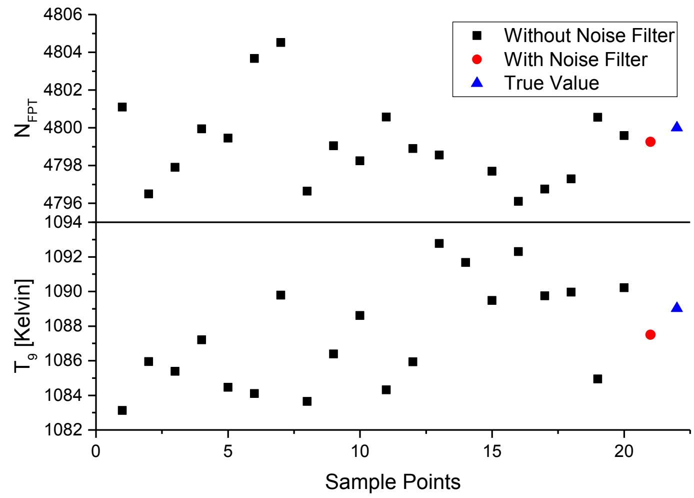

Fig. 10 Measured values of N_{FPT} and T_9 with added Gaussian measurement noise, post-filtered measurement, and true value.

The diagnostic performance of Case 4 is shown in Fig. 11 (a). The relative error of LPT degradation parameters, predicted from the sequential diagnostic with respect to the implanted faults, is shown in Fig. 11 (b). Table 11 indicates that the noisy measurements impact the prediction of the degradation factors when comparing with FPT fault diagnosis (Step 1) in Case 2. Nevertheless, the estimation errors of the degradation factors are still relatively small and acceptable even when the effect of measurement noise has been considered, with the relative errors of efficiency and flow capacity being 0.11% and 0.16%, respectively.

Table 11 Diagnostic results of Case 4.

Items	Symbols	Units	Step 1
Computation Time	CT	Second	0.011
Measurement Error	$RMSE_{Mea}$	-	2.6E-6
Degradation Factor Error	$RMSE_X$	-	1.4E-3
Operating point	n	-	1
No. of Iteration Steps	NIS	-	6
No of total calls to engine sub-models	NO_{Model}	-	18

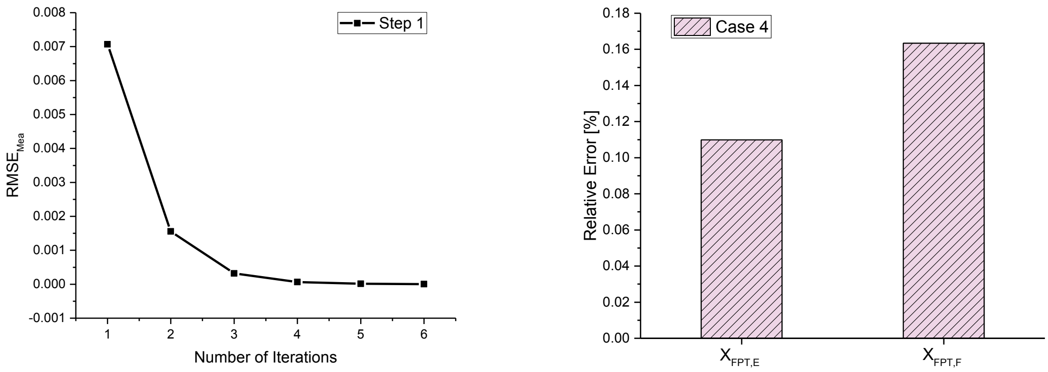

(a) Convergence of diagnosis. (b) Relative diagnostic error.

Fig. 11 Convergence performance and relative diagnostic error for Case 4.

From a practical point of view, several aspects should be taken into consideration in the application of the proposed diagnostic method. Ensuring appropriate systems and support of data filtration [52] and sensor validation [53] should be a priority for fault diagnosis. There is, therefore, a definite need for map adaptation [8,54] of the engine model to align with actual engine measurements based on healthy data and generic maps from the open literature. This adaptation process should be carried out every time maintenance is carried out. This is crucial in refining and updating the engine model that establishes the benchmark upon which any further diagnostic analysis is going to be based. The proposed diagnostic method is not only adequate for off-line steady-state diagnosis but can also be applied in real-time since the fast convergence of the algorithms provides flexibility in its implementation. The comparison between Case 2 and Case 3 reveals that the sequential diagnostic scheme should be reconfigured when there are changes in the type of engine, location of sensors and the number of available sensors. This is a typical limitation from a modeling perspective and something that characterizes the model-based diagnostics methods, which rely heavily on the engine model. However, the substantial accuracy and efficiency improvements of this method, in comparison to existing model-based techniques [45], trade-off the previous limitation.

The findings of this study have several practical implications. More broadly, to develop a full picture of condition-based maintenance, additional studies such as fault prognosis [11,37,55], maintenance optimization [56], economic analysis [57], engine emissions modeling [58] could be implemented to complement the developed model. Further studies, which take these aspects into account, should enable a prognostic health management solution for the gas turbine engine. It will not only improve the reliability and availability of gas turbines but also economically benefit engine stakeholders. The desirable features and excellent performance capabilities of the proposed method motivate the inclusion of transient operating conditions in the diagnosis and variable geometry of compressors; tasks that the authors are currently engaged in.

5. Conclusions

This study proposes a novel sequential diagnostic method for gas turbines with the primary aim of improving the accuracy and computation speed when compared with the conventional model-based GPA. The engine performance model is validated against commercial software for both the design point and off-design steady-state conditions. The novel sequential diagnosis approach is evaluated via a well-used GPA method.

The conclusions drawn from this study are summarized as follows:

- The maximum relative errors between the developed engine performance model and GasTurb is less than 0.71% for the given test conditions.
- The developed sequential diagnostic algorithm is superior in both diagnostic accuracy and computation speed to the conventional GPA, with a maximum relative error less than 1.4E-3 % and convergence in 0.070 seconds.
- The sequential diagnostic algorithm with reduced number of engine measurements outperforms the conventional method. In such a case, the maximum relative error is only 2.2E-2 %, which is significantly lower than the one achieved by the existing NLGPA method. Additionally, the proposed method converges more than 200 times faster than the NLGPA.

- With the aid of a noise filter, the impact of measurement uncertainty can be reduced to an acceptable level for engineering applications. In this situation, the relative errors of two degradation factors for the free power turbine are 0.11% and 0.16% for efficiency and mass flow capacity, respectively.

The present study establishes a sequential framework for engine performance diagnosis with better precision and computation efficiency than the existing model-based method, by eliminating the smearing effect and reducing the matrix dimensions in the iterative diagnostic algorithm. Additionally, the novel diagnostic method with reduced measurement could potentially decrease the cost of engine operations and the flow disturbances caused by sensors in the engine gas path.

Overall, the results of the case studies demonstrate the superiority of this method in terms of diagnostic accuracy and computation time, even with a reduced number of measurements, in comparison with the existing NLGPA method. This new approach is sufficiently modular to be applied in all types of gas turbine engines with the potential to support the operation and maintenance of gas turbine assets more cost-effectively and accurately than existing GPA methods.

Acknowledgments

This work is supported by the Fundamental Research Funds for the Central Universities under Grant No. DUT19ZD218, the National Natural Science Foundation of China under Grant Nos. 61722302 and 61573069.

Appendix A

A.1 Computation Efficiency

This appendix provides detailed information about the iterative diagnostic algorithm from a computational perspective. The sub-model of engine performance simulation consumes most of the computational resources during GPA. The conventional diagnostics covers the “outer loop” (NLGPA: iteration of the degradation factor) and “inner loop” (iteration of the engine performance model). The size of the Jacobian matrix, involved in the iteration, influences the computation speed.

Fig. A. 1 demonstrates the dimensions of the Jacobian matrix for the outer and inner loops of the conventional method [45]. The traditional diagnostic method includes 11 gas path measurements and 10 health parameters (Table

2), which establish the dimensions of the matrix in Fig. A. 1 (pictured at right). The subscript "n" denotes the number of operating points that determine the number of calls to the engine model. In this study, "n" is set to one, two, and three, which correspond to a maximum of 3 operating points. As far as off-design performance is concerned, the developed model needs 8 iteration variables (Appendix B), and the dimension of the matrix for engine simulation are shown in Fig. A. 1. Such a nested iteration reduces the computational efficiency of the engine diagnosis dramatically and could be affected by the smearing effect. The number of calls to the engine model in the diagnostic algorithm and the number of calls to the engine sub-models in engine simulation for one step is also demonstrated in Fig. A. 1.

Conventional Fault Diagnosis Matrix — *Engine Simulation Matrix*

$$\begin{pmatrix} \frac{\partial f_1(\vec{x})}{\partial x_1} & \cdots & \frac{\partial f_1(\vec{x})}{\partial x_{10}} \\ \vdots & \ddots & \vdots \\ \frac{\partial f_{n\cdot 11}(\vec{x})}{\partial x_1} & \cdots & \frac{\partial f_{n\cdot 11}(\vec{x})}{\partial x_{10}} \end{pmatrix}_{n\cdot 11\times 10} \overset{\curvearrowright}{\times} \begin{pmatrix} \frac{\partial f_1(\vec{x})}{\partial x_1} & \cdots & \frac{\partial f_1(\vec{x})}{\partial x_8} \\ \vdots & \ddots & \vdots \\ \frac{\partial f_8(\vec{x})}{\partial x_1} & \cdots & \frac{\partial f_8(\vec{x})}{\partial x_8} \end{pmatrix}_{8\times 8}$$

Call Engine model ×10 ×n
n=1,2,3.

Call Intake, LPC, HPC, Burner, 2 · Mixture, HPT, LPT, FPT, Duct, and Nozzle model ×8

Fig. A. 1 Matrix dimensional analysis of conventional fault diagnosis.

FPT Diagnosis Matrix — *HPC Diagnosis Matrix* — *LPC Diagnosis Matrix* — *HPT and LPT Diagnosis Matrix*

$$\begin{pmatrix} \frac{\partial f_1(\vec{x})}{\partial x_1} & \frac{\partial f_1(\vec{x})}{\partial x_2} \\ \frac{\partial f_2(\vec{x})}{\partial x_1} & \frac{\partial f_2(\vec{x})}{\partial x_2} \end{pmatrix}_{2\times 2} \overset{\Rightarrow}{+} \begin{pmatrix} \frac{\partial f_1(\vec{x})}{\partial x_1} & \frac{\partial f_1(\vec{x})}{\partial x_2} \\ \frac{\partial f_2(\vec{x})}{\partial x_1} & \frac{\partial f_2(\vec{x})}{\partial x_2} \end{pmatrix}_{2\times 2} \overset{\Rightarrow}{+} \begin{pmatrix} \frac{\partial f_1(\vec{x})}{\partial x_1} & \frac{\partial f_1(\vec{x})}{\partial x_2} \\ \frac{\partial f_2(\vec{x})}{\partial x_1} & \frac{\partial f_2(\vec{x})}{\partial x_2} \end{pmatrix}_{2\times 2} \overset{\Rightarrow}{+} \begin{pmatrix} \frac{\partial f_1(\vec{x})}{\partial x_1} & \cdots & \frac{\partial f_1(\vec{x})}{\partial x_7} \\ \vdots & \ddots & \vdots \\ \frac{\partial f_9(\vec{x})}{\partial x_1} & \cdots & \frac{\partial f_9(\vec{x})}{\partial x_7} \end{pmatrix}_{9\times 7}$$

Call FPT model ×2 — *Call HPC model ×2* — *Call LPC model ×2* — *Call HPT, Mixture, LPT model ×7 ×n*
n=3

Fig. A. 2 Matrix dimensional analysis of sequential diagnostic with all available measurements.

Contrary to the conventional method, the sequential diagnostic method needs to call only the specific sub-model directly in the engine performance model, which can reduce computing complexity. Furthermore, the sequential diagnosis has a lower number of matrix dimensions during iteration, which could diminish issues of dimensionality. The size of the Jacobian matrix for the novel sequential approach is also highlighted, and the number of calls to each engine sub-model during one iteration is demonstrated. For sequential diagnostics with all available measurements, the number of dependent variables, independent variables, and calls to engine sub-models are summarized in Fig. A. 2 based on Fig. 3. The number of iteration variables is the longitudinal length of four matrices, which are 2, 2, 2, and

7 for each sequential step in order, respectively. In contrast, the convergence criteria are the transverse length of four matrices, which are 2, 2, 2, and 9, respectively.

For sequential diagnostics with reduced measurements, the number of dependent variables, independent variables, and calls to engine sub-models are summarized in Fig. A. 3, based on Fig. 4. The number of iteration variables is the longitudinal length of three matrices, which are 2, 7, and 7 for each sequential step in order, respectively. In contrast, the convergence criteria are the transverse length of three matrices, which are 3, 9, and 9, respectively. The comparison between the conventional method and novel method on the computation burden is illustrated in Table A. 1. As the actual computation burden relies on the convergence steps, all results presented in Table A. 1 are referred to a single iteration step for obtaining the Jacobian matrix.

FPT Diagnosis Matrix | *HPC and LPC Diagnosis Matrix* | *HPT and LPT Diagnosis Matrix*

$$\begin{pmatrix} \frac{\partial f_1(\vec{x})}{\partial x_1} & \frac{\partial f_1(\vec{x})}{\partial x_2} \\ \vdots & \vdots \\ \frac{\partial f_3(\vec{x})}{\partial x_1} & \frac{\partial f_3(\vec{x})}{\partial x_7} \end{pmatrix}_{3\times 2} \overset{\Rightarrow}{+} \begin{pmatrix} \frac{\partial f_1(\vec{x})}{\partial x_1} & \cdots & \frac{\partial f_1(\vec{x})}{\partial x_7} \\ \vdots & \ddots & \vdots \\ \frac{\partial f_9(\vec{x})}{\partial x_1} & \cdots & \frac{\partial f_9(\vec{x})}{\partial x_7} \end{pmatrix}_{9\times 7} \overset{\Rightarrow}{+} \begin{pmatrix} \frac{\partial f_1(\vec{x})}{\partial x_1} & \cdots & \frac{\partial f_1(\vec{x})}{\partial x_7} \\ \vdots & \ddots & \vdots \\ \frac{\partial f_9(\vec{x})}{\partial x_1} & \cdots & \frac{\partial f_9(\vec{x})}{\partial x_7} \end{pmatrix}_{9\times 7}$$

Call FPT model × 2 × n, *n =3* | *Call LPC and HPC model ×7×n*, *n =3* | *Call HPT, Mixture and LPT model ×7 ×n*, *n=3*

Fig. A. 3 Matrix dimensional analysis of sequential diagnostic with reduced number of measurements.

Table A. 1 Comparison of computation burden to each engine sub-model.

Item	Symbol	CD	SDA	SDR
No. of Calls to Intake Model	NO_{INT}	n ×80	0	0
No. of Calls to Compressor Model	NO_{COP}	n ×160	4	42
No. of Calls to Burner Model	NO_{Burn}	n ×80	0	0
No. of Calls Mixture Model	NO_{MIX}	n ×160	21	21
No. of Calls to Turbine Model	NO_{TURB}	n ×240	44	48
No. of Calls to Duct Model	NO_{DUCT}	n ×80	0	0
No. of Calls to Nozzle Model	NO_{Nozzle}	n ×80	0	0

CD: Conventional Diagnostic.
SDA: Sequential Diagnostic with All Available Measurements.
SDR: Sequential Diagnostic with Reduced Number of Measurements.

Appendix B

B.1 Modular Modelling of Gas Turbine Components

For an industrial gas turbine, the engine consists of six major components: intake, compressor, burner, mixture, turbine, duct, and exhaust nozzle. The algorithm of engine performance simulation was adapted from the method described by [59–63].

- *Intake Model*

For a stationary gas turbine engine, the engine Mach Number is zero, and it is assumed that the engine is installed at sea level with no pressure loss at the intake. Hence, the modeling of intake only needs to decide the WAR for calculating the gas properties at the following simulation. The WAR is calculated by Eq. **(B.1)** [63].

$$WAR = \frac{W_{WA}}{W_{DA}} = \frac{0.622P_{sat}}{\frac{P_{amb}}{0.01RH} - P_{sat}} \quad \textbf{(B.1)}$$

where W_{WA} is mass flow rate of water vapor, W_{DA} denotes the mass flow rate of dry air and P_{sat} denotes the saturation pressure of water vapor.

P_{sat} is obtained by Eq. **(B.2)**, which is related to the ambient pressure and temperature [64].

$$P_{sat} = (1.0007 + 3.46 \cdot 10^{-6} \cdot 101.325P_{amb}) \cdot 0.61121 \cdot exp\left[\frac{17.502(T_{amb} - 273.15)}{T_{amb} - 32.18}\right] \quad \textbf{(B.2)}$$

- *Compressor Model*

For calculating compressor performance, the inlet temperature (T_{in}), pressure (P_{in}), shaft rotational speed (N), compressor flow capacity degradation factor ($X_{C,F}$), and the efficiency degradation factor ($X_{C,E}$) should be known so that the $X_{C,F}$ and $X_{C,E}$ are applied to scale the healthy compressor map by Eq. **(1)**, where $X_{C,F}$ and $X_{C,E}$ are equal to one at a healthy/clean state.

When shaft speed N and inlet conditions are known, the corrected shaft rotational speed (CN) is expressed by Eq. **(B.3)** [60,61].

$$CN = \frac{(N/\sqrt{T_{in}})_{OD}}{(N/\sqrt{T_{in}})_{DP}} \quad \textbf{(B.3)}$$

where the subscript "DP" and "OD" represents the design point and off-design point, respectively.

If the compressor pressure ratio (PR) is known, then the outlet pressure (P_{out}) is determined by:

$$P_{out} = P_{in} \cdot PR \qquad \textbf{(B.4)}$$

As CN and PR are known, the compressor efficiency (Eff_C) and corrected mass flow (CM) could be obtained from the scaled component map. The inlet temperature, pressure, and flow capacity are known, hence the inlet mass flow (W_{in}) is given by:

$$W_{in} = CM \cdot \frac{P_{in}/P_{SLS}}{\sqrt{T_{in}/T_{SLS}}} \qquad \textbf{(B.5)}$$

where the subscript "SLS" represents the sea level static conditions.

The inlet entropy and enthalpy of the compressor are obtained as follows:

$$[S_{in}, H_{in}] = GasProp_{[T,P]}(T_{in}, P_{in}, FAR, WAR) \qquad \textbf{(B.6)}$$

Hence, the enthalpy at isentropic compression (H_{is}) is given by:

$$H_{is} = GasProp_{[S,P]}(S_{in}, P_{out}, FAR, WAR) \qquad \textbf{(B.7)}$$

And the outlet enthalpy is given by Eq. **(B.8)** [59] as follows:

$$H_{out} = H_{in} - (H_{in} - H_{is}) \cdot Eff_C \qquad \textbf{(B.8)}$$

Then, the outlet temperature (T_{out}) can be determined by the following relationship:

$$T_{out} = GasProp_{[H,P]}(H_{out}, P_{out}, FAR, WAR) \qquad \textbf{(B.9)}$$

The calculation of bleeding in a compressor is based on modularizing computations; as demonstrated below for one bleeding path. The required inputs for bleeding include the bleed pressure ratio fraction ($Frac_{PR}$) and bleed mass flow rate fraction ($Frac_W$).

Then, the bleed outlet pressure (PR_{bleed}) and mass flow rate (W_{bleed}) are computed by Eqs. **(B.10)**, **(B.4)** and **(B.11)**:

$$PR_{bleed} = PR \cdot Frac_{PR} \qquad \textbf{(B.10)}$$

$$W_{bleed} = W_{in} \cdot Frac_W \qquad \textbf{(B.11)}$$

Hence, the bleeding outlet enthalpy (H_{bleed}) and temperature (T_{bleed}) are determined by Eqs. **(B.7)**, **(B.8)** and **(B.9)**, respectively.

The outlet mass flow (W_{out}) is calculated by:

$$W_{out} = W_{in} - W_{bleed} \tag{B.12}$$

Finally, the compressor work (CW) is:

$$CW = W_{out} \cdot (H_{out} - H_{in}) + W_{bleed} \cdot (H_{bleed} - H_{in}) \tag{B.13}$$

➢ *Burner Model*

The burner pressure drop (ΔP) can be obtained by Eq. **(B.14)**, which relates the specified design point pressure loss and kinetic head (KH) of burner inlet at both design point and off-design point conditions [62]:

$$\frac{\Delta P_{DP}}{\Delta P_{OD}} = \frac{KH_{DP}}{KH_{OD}} \tag{B.14}$$

where the kinetic head is referred to Eq. **(B.15)** as follows:

$$KH = \frac{W_{in}^2 \cdot T_{in}}{P_{in}} \tag{B.15}$$

The burner exit pressure is computed by:

$$P_{out} = P_{in} \cdot \Delta P_{OD} \tag{B.16}$$

The enthalpy released (ΔH) by fuel combustion is given by:

$$\Delta H = W_{Fuel} \cdot LHV \cdot Eff_B \tag{B.17}$$

where W_{Fuel} is the burner fuel flow rate, LHV is low heating value, and Eff_B is burner efficiency.

The computation of the exit enthalpy of combustion gas is based on mass and energy conservation:

$$H_{out} = \frac{H_{in} \cdot W_{in} + \Delta H}{W_{out}} \tag{B.18}$$

The FAR of the combustor gas is determined through WAR, W_{Fuel} and W_{out} as follows:

$$FAR = \frac{W_{Fuel}}{(W_{out} - W_{Fuel}) \cdot (1 - WAR)} \tag{B.19}$$

Finally, the burner exit temperature is obtained by Eq. **(B.9)**.

➢ *Mixture Model*

The mixture model is applied for mixing of core flow, and cooling flows in a constant area, when one inlet flow is much smaller than the other. It is assumed that the total outlet pressure of mixed flow is equal to the total inlet pressure of core flow. The mass flow of mixed flow can be determined based on mass conservation. Then, the enthalpy of exit is:

$$H_{out} = \frac{W_{main} \cdot H_{main} + W_{bleed} \cdot H_{bleed}}{W_{out}} \quad \textbf{(B.20)}$$

Finally, the FAR of mixed gas is referred to Eq. **(B.19)** and the outlet temperature of mixed flow is determined by Eq. **(B.9)**.

➢ *Turbine Model*

For calculating the turbine performance model, the T_{in}, P_{in}, N, W_{Fuel}, turbine flow capacity degradation factor $X_{T,F}$, and turbine efficiency degradation factor $X_{T,E}$ should be known and $X_{T,F}$ are $X_{T,E}$ are applied to scale the original health map by Eq. **(1)**, where $X_{T,F}$ and $X_{T,E}$ are equal to one at a healthy/clean state.

When shaft speed N and the inlet conditions are known, the CN could be obtained by Eq. **(B.3)**. If the turbine expansion ratio of pressure (PR) is known, the turbine outlet pressure (P_{out}) is given by:

$$P_{out} = P_{in}/PR \quad \textbf{(B.21)}$$

As CN and PR are known, the actual turbine efficiency (Eff_T) and corrected mass flow (CM) could be obtained from the scaled turbine map. Due to the turbine inlet temperature, pressure, and corrected mass flow are known, the turbine inlet mass flow could be obtained by Eq. **(B.5)**.

Since the Eff_T is known, the turbine outlet enthalpy is computed by:

$$H_{out} = H_{in} - (H_{in} - H_{is}) \cdot Eff_T \quad \textbf{(B.22)}$$

The turbine outlet temperature could be calculated by Eq. **(B.9)**, and turbine work (TW) is as follows:

$$TW = W_{in} \cdot (H_{in} - H_{out}) \quad \textbf{(B.23)}$$

➢ *Duct Model*

In the Duct model, we considered a total pressure loss that could be obtained by Eq. **(B.14)**. The outlet mass flow and total enthalpy are the same as the inlet condition. Hence, the outlet temperature is calculated by Eq. **(B.9)**.

➢ *Nozzle Model*

For industrial gas turbines, the Mach number of nozzle exit flow is less than one since the nozzle is under sub-critical condition. Hence, the following calculation will only discuss the calculation process for subsonic flow where the nozzle exit static pressure (p_{out}) is equal to the ambient pressure. Moreover, the assumed isentropic expansion means that the static entropy (s_{out}) is equal to total entropy (S_{out}) and obtained by Eq. **(B.6)**. The nozzle static temperature (t_{out}), static density (ρ_{out}), heat capacity ratio (γ), and gas constant (R_g) are given by:

$$[t_{out}, \rho_{out}, \gamma, R_g] = GasProp_{[S,P]}(s_{out}, p_{out}, FAR, WAR) \quad \textbf{(B.24)}$$

Then, the nozzle outlet velocity (V_{out}) is calculated by:

$$V_{out} = \sqrt{\gamma \cdot R_g \cdot t_{out}} \quad \textbf{(B.25)}$$

Finally, the determination of the nozzle exit mass flow is based on the component characteristic.

$$W_{out} = \rho_{out} \cdot V_{out} \cdot A_{out} \quad \textbf{(B.26)}$$

where A_{out} is the cross-section area of the exhaust nozzle.

B.2 Map Scaling of Rotating Component at Design Point

The rotating component maps include the characteristic parameters, such as corrected shaft rotational speed, pressure ratio, corrected mass flow rate, and component efficiency. However, the generic maps from the open literature may not align with actual component characteristics in concern at the design point. Hence, the design point map scaling is launched and referred to [46] to represent the actual component characteristic based on the design point specification.

The scaling factor of pressure ratio (SF_{PR}) is:

$$SF_{PR} = \frac{PR_{DP} - 1}{PR_{map} - 1} \quad \textbf{(B.27)}$$

where the subscript "DP" refers to the design point value, while the subscript "map" indicates the value obtained through generic maps.

The scaling factor of corrected mass flow (SF_{CM}) is given by:

$$SF_{CM} = CM_{DP}/CM_{map} \quad \textbf{(B.28)}$$

Similarly, the scaling factor of component efficiency (SF_{Eff}) is:

$$SF_{Eff} = Eff_{DP}/Eff_{map} \quad \textbf{(B.29)}$$

B.3 Cross-Section Area of Exhaust Nozzle

For the design point, the nozzle exit entropy could be obtained by Eq. **(B.6)**. By assuming that the exhaust gas is expanding isentropically [63] to the ambient, the static entropy (s_{out}) is equal to the total entropy (S_{out}). Hence, t_{out}, ρ_{out}, γ and R_g are calculated by Eq. **(B.24)** and the V_{out} is given by Eq. **(B.25)**.

Finally, the exhaust nozzle's cross-section area is determined by Eq. **(B.30)**, while exhaust mass flow rate is known at the design point.

$$A_{out} = W_{out}/(\rho_{out} \cdot V_{out}) \quad \textbf{(B.30)}$$

B.4 Gas Turbine Performance Model for RB211-24G

The gas turbine's performance simulation is based on the above algorithms for each engine component representing any gas turbine. The balancing process of a triple-shaft industrial gas turbine engine is shown in Fig. B. 1 which is adapted from [40]. Eight iteration variables are required for the iteration that are N_{LP}, PR_{LPC}, N_{HP}, PR_{HPC}, W_{Fuel}, PR_{HPT}, PR_{LPT}, PR_{FPT}. Meanwhile, convergence criteria are shown in the left part of Fig. B. 1, where the subscript "pre" refers to the mass flow from the previous block. In contrast, the subscript "loc" indicates the mass flow obtained through component characteristics.

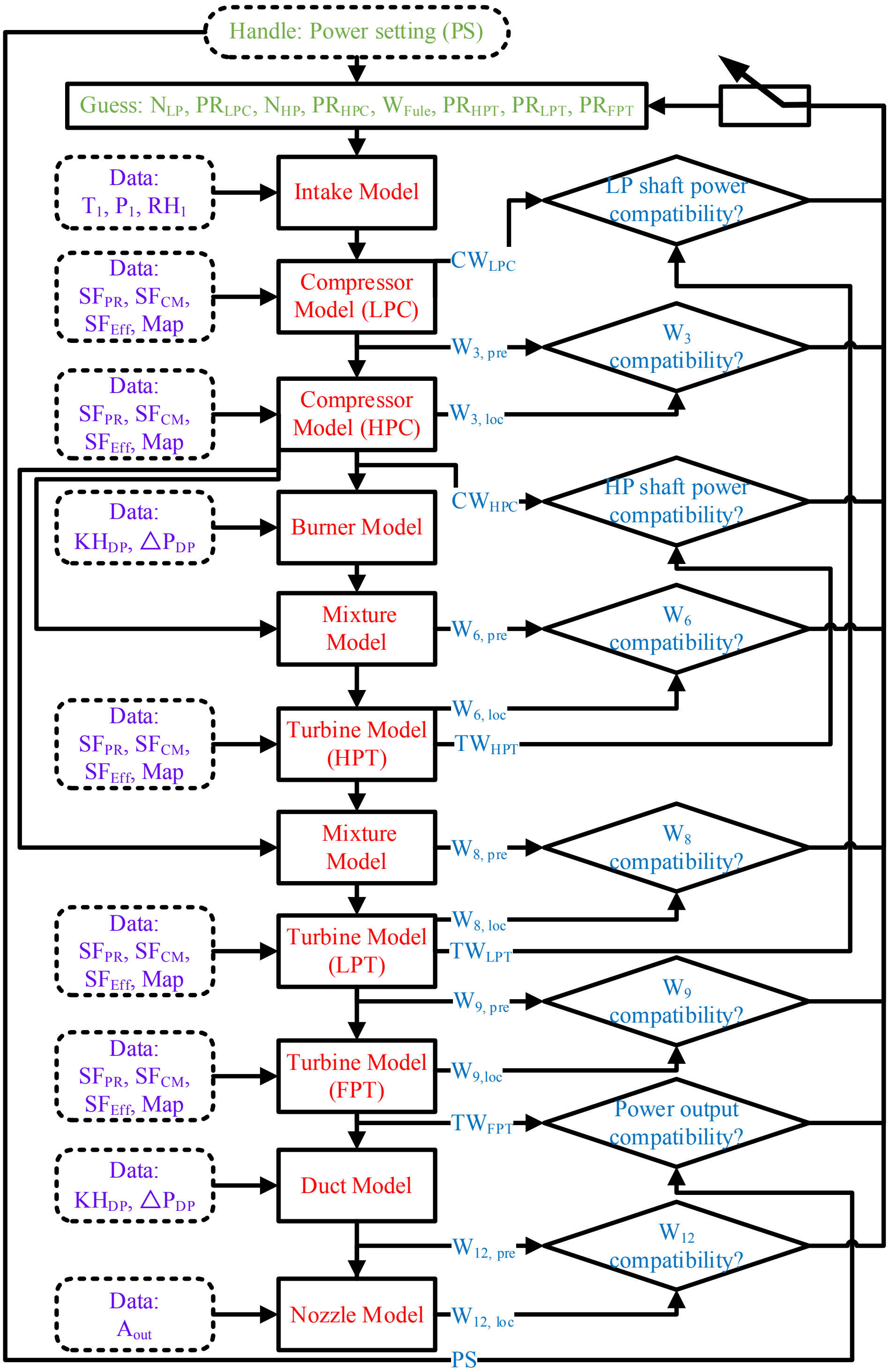

Fig. B. 1 Balancing process of the off-design performance simulation.

References

[1] Tahan M, Tsoutsanis E, Muhammad M, Abdul Karim ZA. Performance-based health monitoring, diagnostics and prognostics for condition-based maintenance of gas turbines: A review. Appl Energy 2017;198:122–44.

[2] Aminyavari M, Mamaghani AH, Shirazi A, Najafi B, Rinaldi F. Exergetic, economic, and environmental evaluations and multi-objective optimization of an internal-reforming SOFC-gas turbine cycle coupled with a Rankine cycle. Appl Therm Eng 2016;108:833–46.

[3] Marinai L, Probert D, Singh R. Prospects for aero gas-turbine diagnostics: A review. Appl Energy 2004;79:109–26.

[4] Hanachi H, Liu J, Kim IY, Mechefske CK. Hybrid sequential fault estimation for multi-mode diagnosis of gas turbine engines. Mech Syst Signal Process 2019;115:255–68.

[5] Talebi SS, Tousi AM. The effects of compressor blade roughness on the steady state performance of micro-turbines. Appl Therm Eng 2017;115:517–27.

[6] Urban LA. Gas Turbine Engine Parameter Interrelationships. 2nd ed. Hamilton Standard Division of United Aircraft Corporation; 1969.

[7] Safiyullah F, Sulaiman SA, Naz MY, Jasmani MS, Ghazali SMA. Prediction on performance degradation and maintenance of centrifugal gas compressors using genetic programming. Energy 2018;158:485–94.

[8] Kang DW, Kim TS. Model-based performance diagnostics of heavy-duty gas turbines using compressor map adaptation. Appl Energy 2018;212:1345–59.

[9] Sogut MZ, Yalcin E, Karakoc TH. Assessment of degradation effects for an aircraft engine considering exergy analysis. Energy 2017;140:1417–26.

[10] Hanachi H, Mechefske C, Liu J, Banerjee A, Chen Y. Performance-Based Gas Turbine Health Monitoring, Diagnostics, and Prognostics: A Survey. IEEE Trans Reliab 2018;67:1340–63.

[11] Tsoutsanis E, Meskin N, Benammar M, Khorasani K. A dynamic prognosis scheme for flexible operation of gas turbines. Appl Energy 2016;164:686–701.

[12] Tsoutsanis E, Hamadache M, Dixon R. Real-Time Diagnostic Method of Gas Turbines Operating Under Transient Conditions in Hybrid Power Plants. J Eng Gas Turbines Power 2020;142:1–10.

[13] Orozco DJR, Venturini OJ, Escobar Palacio JC, del Olmo OA. A new methodology of thermodynamic diagnosis, using the thermoeconomic method together with an artificial neural network (ANN): A case study of an externally fired gas turbine (EFGT). Energy 2017;123:20–35.

[14] Tang S, Tang H, Chen M. Transfer-learning based gas path analysis method for gas turbines. Appl Therm Eng 2019;155:1–13.

[15] Korbicz J, Kościelny JM, Kowalczuk Z, Cholewa W. Fault Diagnosis: Models, Artificial Intelligence, Applications. 2th ed. New York, US: Springer; 2012.

[16] Ying Y, Cao Y, Li S, Li J, Guo J. Study on gas turbine engine fault diagnostic approach with a hybrid of gray relation theory and gas-path analysis. Adv Mech Eng 2016;8:1–14.

[17] Fentaye AD, Baheta AT, Gilani SI, Kyprianidis KG. A review on gas turbine gas-path diagnostics: State-of-the-art methods, challenges and opportunities. Aerospace 2019;6.

[18] Hanachi H, Liu J, Mechefske C. Multi-mode diagnosis of a gas turbine engine using an adaptive neuro-fuzzy system. Chinese J Aeronaut 2018;31:1–9.

[19] Simon DL, Rinehart AW. Sensor Selection for Aircraft Engine Performance Estimation and Gas Path Fault Diagnostics. J Eng Gas Turbines Power 2016;138:1–11.

[20] Jasmani MS, Li YG, Ariffin Z. Measurement selections for multi-component gas path diagnostics using analytical approach and measurement subset concept. Proc ASME Turbo Expo 2010;3:569–79.

[21] Pinelli M, Spina PR, Venturini M. Gas turbine health state determination: Methodology approach and field application. Int J Rotating Mach 2012;2012.

[22] Hanachi H, Liu J, Banerjee A, Chen Y, Koul A. A physics-based modeling approach for performance monitoring in gas turbine engines. IEEE Trans Reliab 2015;64:197–205.

[23] Lu F, Ju H, Huang J. An improved extended Kalman filter with inequality constraints for gas turbine engine health monitoring. Aerosp Sci Technol 2016;58:36–47.

[24] Mohammadi E, Montazeri-Gh M. Performance enhancement of global optimization-based gas turbine fault diagnosis systems. J Propuls Power 2016;32:214–24.

[25] Yang Q, Li S, Cao Y, Zhao N. Full and part-load performance deterioration analysis of industrial three-shaft gas turbine based on genetic algorithm. Proc. ASME Turbo Expo, vol. 6, Seoul, South Korea: ASME Turbo Expo 2016: Turbomachinery Technical Conference and Exposition; 2016, p. 1–12.

[26] Sun J, Zuo H, Liang K, Chen Z. Bayesian Network-Based Multiple Sources Information Fusion Mechanism for Gas Path Analysis. J Propuls Power 2016;32:611–9.

[27] Yang Q, Li S, Cao Y. An IMM-GLR Approach for Marine Gas Turbine Gas Path Fault Diagnosis. Math Probl Eng 2018;2018.

[28] Yang Q, Li S, Cao Y. Multiple model-based detection and estimation scheme for gas turbine sensor and gas path fault simultaneous diagnosis. J Mech Sci Technol 2019;33:1959–72.

[29] Cherchi E, Guevara CA. A Monte Carlo experiment to analyze the curse of dimensionality in estimating random coefficients models with a full variance-covariance matrix. Transp Res Part B Methodol 2012;46:321–32.

[30] Lei L, Xu H, Xiong X, Zheng K, Xiang W, Wang X. Multiuser Resource Control With Deep Reinforcement Learning in IoT Edge Computing. IEEE Internet Things J 2019;6:10119–33.

[31] Daroogheh N, Meskin N, Khorasani K. A Dual Particle Filter-Based Fault Diagnosis Scheme for Nonlinear Systems. IEEE Trans Control Syst Technol 2017;26:1317–34.

[32] Tsoutsanis E, Meskin N, Benammar M, Khorasani K. A component map tuning method for performance prediction and diagnostics of gas turbine compressors. Appl Energy 2014;135:572–85.

[33] Yang Q, Li S, Cao Y. A strong tracking filter based multiple model approach for gas turbine fault diagnosis. J Mech Sci Technol 2018;32:465–79.

[34] Lu F, Wang Y, Huang J, Huang Y, Qiu X. Fusing unscented Kalman filter for performance monitoring and fault accommodation in gas turbine. Proc Inst Mech Eng Part G J Aerosp Eng 2018;232:556–70.

[35] John S. Microsoft Visual C# Step by Step. 9 edition. Hoboken, USA: Microsoft Press; 2018.

[36] Sun W. Research on Performance Calculation Model of RB211-24G Gas Turbine. MEng Thesis, China University of Petroleum Beijing, China, 2017.

[37] Tsoutsanis E, Meskin N. Derivative-driven window-based regression method for gas turbine performance prognostics. Energy 2017;128:302–11.

[38] Zhou D, Yao Q, Wu H, Ma S, Zhang H. Fault diagnosis of gas turbine based on partly interpretable convolutional neural networks. Energy 2020;200:117467.

[39] Plis M, Rusinowski H. A mathematical model of an existing gas-steam combined heat and power plant for thermal diagnostic systems. Energy 2018;156:606–19.

[40] Song Y, Gu C, Ji X. Development and validation of a full-range performance analysis model for a three-spool gas turbine with turbine cooling. Energy 2015;89:545–57.

[41] NASA. NASA computer program for calculating of the Chemical Equilibrium with Application, Cleveland, OH: NASA Glenn Research Center 2015.

[42] Li Y-G. Gas Turbine Diagnostics. Cranfield, Bedford, UK: Cranfield University Msc Thermal Power Course Notes; 2019.

[43] SIEMENS Products & Services. SGT-A35 (Industrial RB211) aeroderivative gas turbine 2020. https://new.siemens.com/global/en/products/energy/power-generation/gas-turbines/sgt-a30-a35-rb.html (accessed July 2, 2020).

[44] Kurzke J. GasTurb 13: A Program to Calculate Design and Off-Design Performance of Gas Turbines 2017.

[45] Li J, Ying Y. A Method to Improve the Robustness of Gas Turbine Gas-Path Fault Diagnosis Against Sensor Faults. IEEE Trans Reliab 2018;67:3–12.

[46] Ogaji SOT, Sampath S, Singh R, Probert SD. Parameter selection for diagnosing a gas-turbine's performance-deterioration. Appl Energy 2002;73:25–46.

[47] Li J, Ying Y. Gas turbine gas path diagnosis under transient operating conditions: A steady state performance model based local optimization approach. Appl Therm Eng 2020;170.

[48] Chen YZ, Li YG, Newby MA. Performance simulation of a parallel dual-pressure once-through steam generator. Energy 2019;173:16–27.

[49] Chen YZ, Li YG, Newby MA. Gas path diagnostics for a once-through steam generator. Proc. ASME Turbo Expo, vol. 3, Phoenix, Arizona, USA: 2019, p. 1–11.

[50] Amirkhani S, Chaibakhsh A, Ghaffari A. Nonlinear robust fault diagnosis of power plant gas turbine using Monte Carlo-based adaptive threshold approach. ISA Trans 2019.

[51] Kim P. Kalman filter for beginners: with MATLAB examples. North Charleston, S.C., United States: CreateSpace Independent Publishing Platform; 2011.

[52] Hu RL, Granderson J, Auslander DM, Agogino A. Design of machine learning models with domain experts for automated sensor selection for energy fault detection. Appl Energy 2019;235:117–28.

[53] Palmé T, Fast M, Thern M. Gas turbine sensor validation through classification with artificial neural networks. Appl Energy 2011;88:3898–904.

[54] Kim S, Kim K, Son C. A new transient performance adaptation method for an aero gas turbine engine. Energy 2020;193:116752.

[55] Zagorowska M, Schulze Spüntrup F, Ditlefsen AM, Imsland L, Lunde E, Thornhill NF. Adaptive detection and prediction of performance degradation in off-shore turbomachinery. Appl Energy 2020;268.

[56] Aretakis N, Roumeliotis I, Doumouras G, Mathioudakis K. Compressor washing economic analysis and optimization for power generation. Appl Energy 2012;95:77–86.

[57] Kotowicz J, Brzęczek M, Job M. The thermodynamic and economic characteristics of the modern combined cycle power plant with gas turbine steam cooling. Energy 2018;164:359–76.

[58] Owebor K, Oko COC, Diemuodeke EO, Ogorure OJ. Thermo-environmental and economic analysis of an integrated municipal waste-to-energy solid oxide fuel cell, gas-, steam-, organic fluid- and absorption refrigeration cycle thermal power plants. Appl Energy 2019;239:1385–401.

[59] Linares JI, Montes MJ, Cantizano A, Sánchez C. A novel supercritical CO2 recompression Brayton power cycle for power tower concentrating solar plants. Appl Energy 2020;263:114644.

[60] Bracco S, Delfino F. A mathematical model for the dynamic simulation of low size cogeneration gas turbines within smart microgrids. Energy 2017;119:710–23.

[61] Tsoutsanis E, Meskin N. Dynamic performance simulation and control of gas turbines used for hybrid gas/wind energy applications. Appl Therm Eng 2019;147:122–42.

[62] Kim MJ, Kim JH, Kim TS. The effects of internal leakage on the performance of a micro gas turbine. Appl Energy 2018;212:175–84.

[63] Kurzke J, Halliwell I. Propulsion and Power: An Exploration of Gas Turbine Performance Modeling. Cham, Switzerland: Springer International Publishing AG, part; 2018.

[64] Buck AL. New equations for computing vapour pressure and enhancement factor. J Appl Meteorol 1981;20:1527–32.